GDCh

Research Article

Angewandte
Chemie
International Edition
www.angewandte.org

Hydrogen-bonded Organic Frameworks

A Simple and Sequential Strategy for the Introduction of Complexity and Hierarchy in Hydrogen-Bonded Organic Framework (HOF) Crystals for Environmental Applications

Christopher A. Halliwell, Kenny Jolley, Keith Yendall, Mark R. J. Elsegood, Gary N. Parkinson,* and Antonio Fernandez*

Abstract: Hydrogen-bonded organic frameworks (HOFs) are a new class of crystalline porous organic molecular materials (POMMs) with great potential for a diverse range of applications. HOFs face common challenges to POMMs, and in general to purely organic crystals, that is, the difficulty of integrating complexity in crystals. Herein, we propose a simple and sequential strategy for the formation of HOFs with hierarchical superstructures. The strategy is based on controlling the assembly conditions, avoiding the use of any surface functionalization or template, which allows to obtain hierarchical crystalline porous superstructures in an easy manner. As proof of concept, we obtained the first example of core–shell (HOF-on-HOF) crystals and HOFs with hierarchical superstructures having super-hydrophobicity and trapping abilities for the capture of persistent water contaminants such as oils and micro-plastics. We expect that this strategy could serve as inspiration for the construction of more intricate multi-scale structures that could greatly expand the library of HOF materials.

[*] Dr. C. A. Halliwell, Dr. K. Jolley, Dr. M. R. J. Elsegood, Dr. A. Fernandez
Chemistry Department, School of Science
Loughborough University, Loughborough, LE11 3TU, UK
E-mail: a.fernandez-mato@lboro.ac.uk

Dr. K. Yendall
School of Aeronautical, Automotive, Chemical and Materials Engineering, (AACME)
Loughborough University, Loughborough, LE11 3TU, UK

Dr. G. N. Parkinson
UCL School of Pharmacy, University College London, London, WC1N 1AX, UK
E-mail: gary.parkinson@ucl.ac.uk

Introduction

Porous organic molecular materials (POMMs) are a new class of synthetic materials characterized by the formation of porous frameworks mainly held together by non-covalent interactions.[1] One type of POMMs are hydrogen-bonded organic frameworks (HOFs), forming porous frameworks held by hydrogen bonds and π–π stacking interactions during crystallization.[2] HOFs have a unique combination of properties such as high crystallinity, high flexibility, lower weight, less inherent toxicity, recyclability, solution process-ability and self-healing properties. Since these properties are complementary to those with covalent and coordinated frameworks such as covalent organic frameworks (COFs)[3] and metal–organic frameworks (MOFs),[4] HOFs are considered excellent candidates for a vast range of applications.[5] A clear evolution in the field of HOFs would be the integration of higher levels of ordered complexity[6,7] or hierarchy,[8–10] during crystallization. Conceptually, by combining these hierarchies in a single material, novel materials with synergistic properties could be obtained, while expanding the number of HOF materials available in the toolbox. However, obtaining hierarchical crystals in purely organic materials[11–14] such as HOFs is quite challenging due to the difficulty of controlling the weak interactions during crystallization, the different chemical stabilities between materials[15] and strict lattice-matching requirements.[16] Herein, we describe a template-free and versatile strategy, based on well controlled sequential crystallization steps from two molecular precursors, to obtain hierarchical HOF superstructures.[17,18] The simple assembly process allows us to obtain the first examples of purely organic HOF super-structures (Figure 1), showing unique features such as hierarchically branched nanostructures and core–shell (HOF-on-HOF) architecture. We based our strategy on the affinity of pyridine and carboxylic acid for the formation of strong hydrogen bonds and the compatibility in solubilities and stabilities between HOF precursors. With this simple strategy, commonly used approaches such as surface functionalization or the use of a template[17,19,20] are not required. The versatile strategy opens the door for the design of HOF-based superstructures with unprecedented complexity.

Angew. Chem. Int. Ed. **2024**, *63*, e202404452 (1 of 7)

© 2024 The Authors. Angewandte Chemie International Edition published by Wiley-VCH GmbH
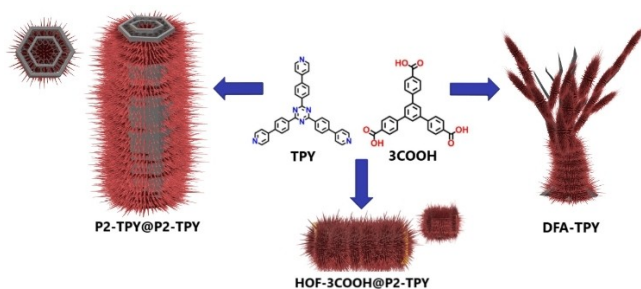
Figure 1. Schematic representation of the crystalline hierarchical super-structures obtained from two molecular precursors.

Results and Discussion

Crystalline Hierarchical Superstructures, DFA-TPY and P2-TPY@P2-TPY

The preparation of **DFA-TPY** (**DFA-TPY**: Double Fractal Architecture-Tripyridine) and **P2-TPY@P2-TPY** (**P2-TPY**: micro-macro Porosity-Tripyridine) starts from precursor **TPY** (Figure 2, Figure S1). The choice of solvent, concentration, and control of the evaporation rate at different stages is fundamental for the obtention of fractal superstructures. Initially, crystalline assemblies of **FA-TPY** (**FA-TPY**: Fractal Architecture-Tripyridine) with millimeter size and fractal-like morphology were obtained from a solution in toluene of **TPY** precursor (>1.2 mg/mL) at low solvent evaporation rate (>3 days). Then, **FA-TPY** was immersed in a solution of **TPY** in toluene (>0.8 mg/mL) and the solvent was left to evaporate at a fast rate (~20 hours) to obtain the final assembly, **DFA-TPY**. The relatively fast nucleation of the smaller crystals, generated on the surface of the main **FA-TPY** crystalline assembly, yields a dense array of crystals. Scanning electron microscopy (SEM) confirmed the multiscale morphology, with a secondary generation of crystals growing at the surface of the larger **FA-TPY** assemblies, having average diameters of less than 1 micrometer (Figure 2c). During the crystallization process and after thermal activation, the crystalline integrity of **DFA-TPY** is maintained, as confirmed by powder X-ray diffraction (PXRD) (Figure S4) and matches with the phase of a recently reported microporous HOF.[21] The thermal stability of the **DFA-TPY** building block was also studied by thermogravimetric analysis (TGA) under N_2 (Figure S5). An initial and gradual 5% weight loss below 300°C was attributed to the loss of toluene within the packing. A second weight loss of >70% between 400°C and 500°C was attributed to the thermal decomposition of **TPY**. This confirms that the **DFA-TPY** precursor is thermally stable below 400°C.

P2-TPY hollow crystals, used for the obtention of **P2-TPY@P2-TPY** (Figure 3), were also prepared from precursor **TPY** but at low concentration (<0.6 mg/mL) and low evaporation rate of toluene (>4 days). SEM images of the crystals revealed macropores within the main hollow interior (Figure 3b). The crystal structure of **P2-TPY** was solved by SCXRD analysis (Table S1). In the crystal packing, there are six **TPY** molecules and nine toluene molecules in the asymmetric unit. The packing is represented by the **TPY** molecules arranged in pairs and all six unique molecules forming an infinite $\pi\cdots\pi$ stacked column parallel to b (Figure 3d). The first molecule is adjacent to a symmetry equivalent of the sixth molecule. The closest contacts between atoms of central rings are significantly shorter than usual $\pi\cdots\pi$ stacking distances, between 3.26–3.35 Å. The spread of the centroid-centroid distances and pattern of closest contacts supports the monoclinic space group selection due to the pattern of variation. If the **TPY**
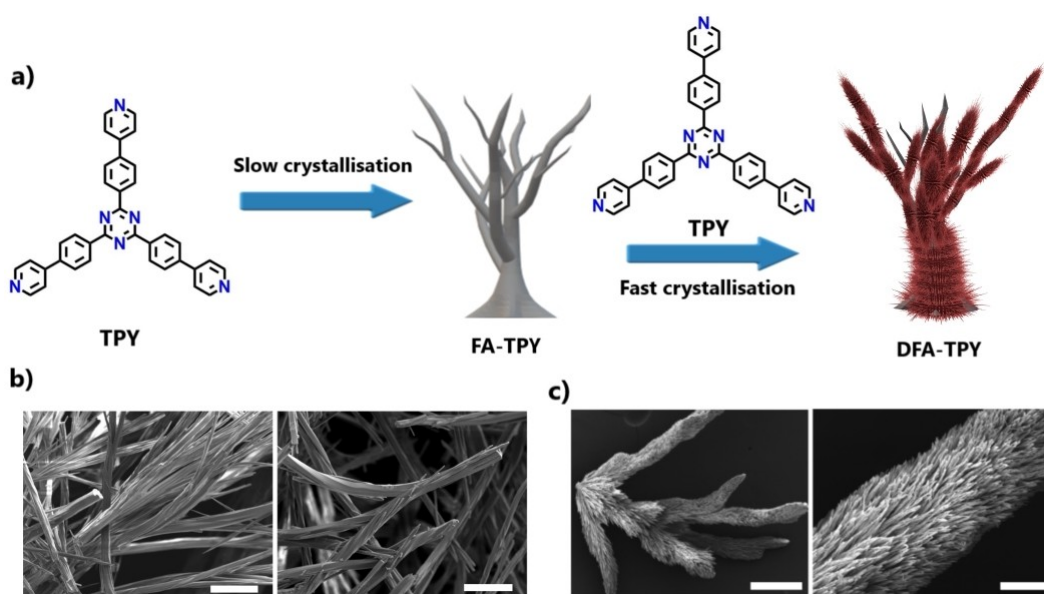

Figure 2. a) Schematic representation of the sequential crystallization of **FA-TPY** and **DFA-TPY**. b-c) SEM images of **FA-TPY** (b) and **DFA-TPY** (c). Scale bars (from left to right): (b) 100 μm, 100 μm, (c) 100 μm, 10 μm.
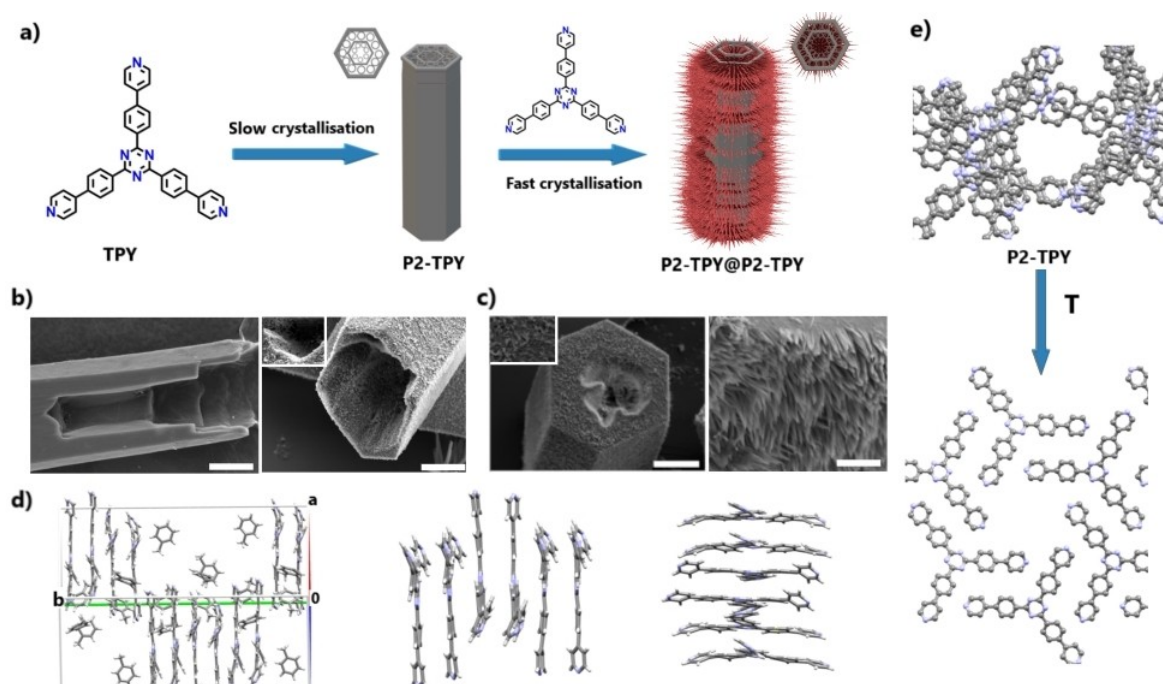
Figure 3. a) Schematic representation of the sequential crystallization of **P2-TPY@P2-TPY**. b–c) SEM images of **P2-TPY** (b Right) and **P2-TPY@P2-TPY** ((b Left), c). d) Crystal packing obtained from single crystal X-ray of **P2-TPY**, with different views of the molecular interactions in the packing arrangement showing the strong, slightly slipped π–π stacking. Blue: N, Grey: C. e) Changes in the crystal packing of **P2-TPY** (single-crystal to single-crystal transformation) to the same phase as **DFA-TPY**, previously reported.[21] Scale bars (from left to right): (b) 10 μm, (c) 10 μm (Left), 1 μm (Right). Hydrogens have been omitted for clarity.

molecules are regarded as being arranged in layers in the *a/c* plane, then the toluene molecules are in the formed cavity between every other layer in the spaces between stacks of molecules. There is no additional void volume or disorder. With the toluene molecules removed, there are three unique 'voids', so six in total in the unit cell. Each equates to about 5 % of the cell volume. The void volumes for each individual void are: 538, 545, and 530 Å^3. Overall ca. 30 % of the cell volume is occupied by toluene molecules, thus defining the presence of micropores where the longest diagonal distance within each pore is close to 1.6 nm. Next, crystals of **P2-TPY** with micrometer size (Figure 3a), initially having hierarchical micro and macroporosity, were immersed in a solution of **TPY** precursor in toluene (<0.6 mg/mL) and the solvent was left to evaporate at a fast rate (~20 minutes). The relatively fast nucleation of the newly generated smaller crystals of **P2-TPY** on the surface of the main hollow **P2-TPY** crystals yields a dense array of nanocrystals with average diameters of 100–200 nm, covering most of the surface of the main hollow crystal, including the inner main hollow structure, thus forming superstructures with hierarchical architecture and porosity. SEM confirmed that the secondary generation of **P2-TPY** nanocrystals growing at the surface of larger crystals have rod morphology (Figure 3b) forming a multiscale morphology that resembles a nanoforest. This strategy is also versatile in terms of scale. For example, by modifying the size of the seed crystals of **P2-TPY**, from micrometer to millimeter size, a secondary generation of micrometer size crystals can be grown, which

can be easily visualized by optical microscopy (Figure S6). During the crystallization process for the formation of **P2-TPY@P2-TPY** with hierarchical porosity and hierarchical architecture, the crystalline integrity of **P2-TPY** is maintained, as confirmed by powder X-ray diffraction (PXRD) (Figure S7). However, during the activation of **P2-TPY@P2-TPY** at 110 °C, single-crystal to single-crystal transformation occurred to form a new crystalline microporous phase, matching with the **DFA-TPY** phase (Figure 3d). The thermal stability of **P2-TPY@P2-TPY** was studied by TGA, confirming similar stability to **DFA-TPY** (Figure S8).

Crystalline Core-Shell Superstructures (HOF-on-HOF), HOF-3COOH@P2-TPY

First, crystals of **HOF-3COOH** were obtained from slow crystallization (~2 weeks) of a methanol solution of **3COOH** (~1.4 mg/mL) precursor at room temperature (Figure 4). SCXRD was used to determine the crystal packing of **HOF-3COOH** (Table S2). Packing in the unit cell is accommodated by both ring π–π stacking and the interlocking together of the **3COOH** molecules, dominated by hydrogen bonding involving all three carboxyl COOH groups (Figure 4b). The rotatable bond of the carboxylic acid allows for two possible hydrogen bonding orientations in the crystal lattice seen here, generating an average bond length for OH carboxyl donor atoms. The **3COOH** molecules interact through π···π stacking of the central aromatic ring as a
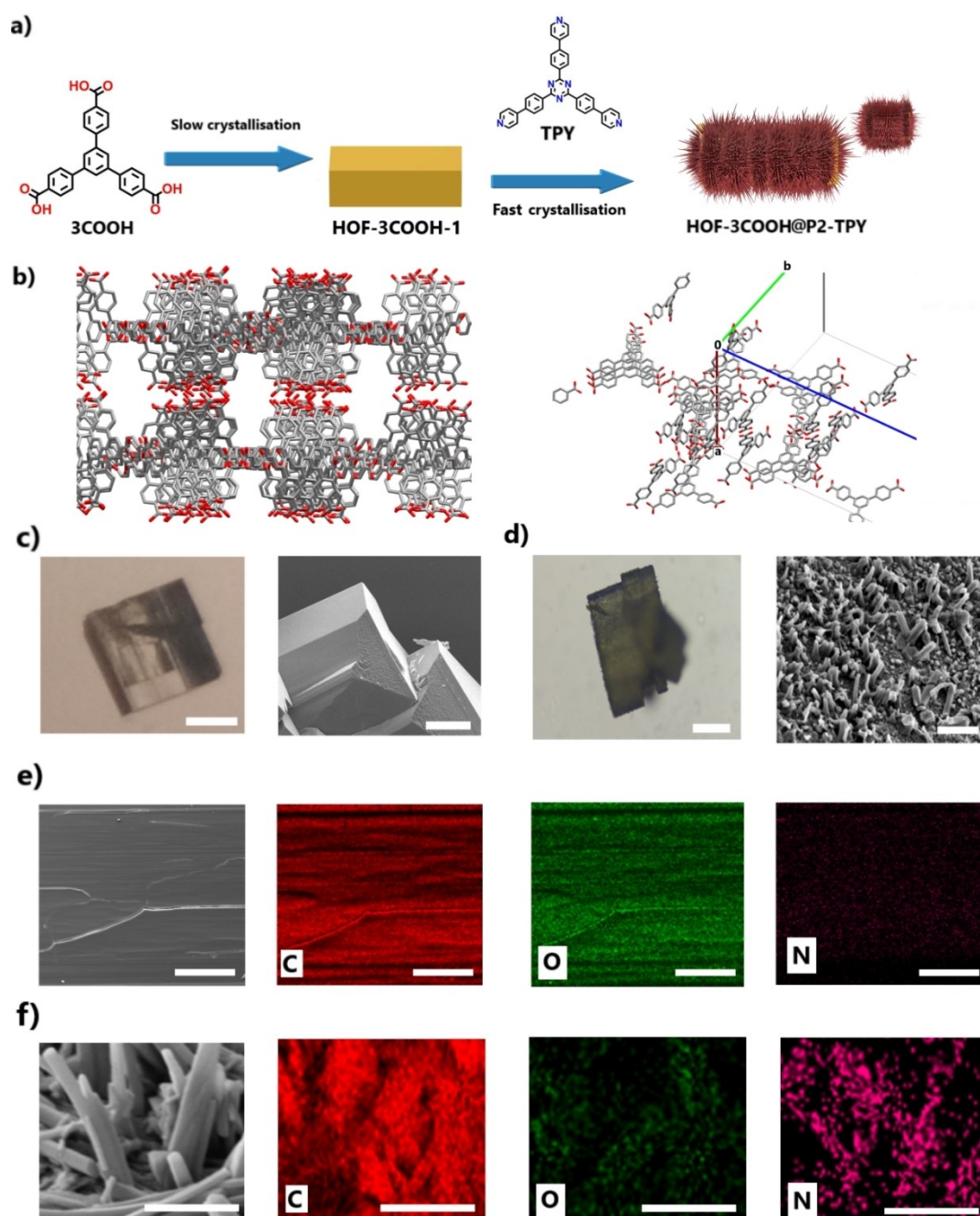
Figure 4. a) Schematic representation of the sequential crystallization of **HOF-3COOH@P2-TPY**. b) Different views of the crystal packing of **HOF-3COOH** showing the channels and the molecular interactions in the packing arrangement with the strong COOH-COOH H-bonds and π–π stacking and the asymmetric unit. Red: O, Grey: C. All hydrogens have been omitted for clarity. c-d) Optical (Left) and SEM (Right) images of **HOF-3COOH** (c) and **HOF-3COOH@P2-TPY** (d). e–f) EDS mapping of C, O and N for **HOF-3COOH** (e) and **3COOH@P2-TPY** (f Scale bars (from left to right): (c) 100 μm, (d) 50 μm, 1 μm, (e) 10 μm, (f) 1 μm.

column consisting of sets four molecules plus three molecules, packed as a herringbone arrangement resulting in twenty-eight (4×7) independent molecules in the ASU. The total solvent-accessible volume is 29404 Å³ made from four equivalent 'voids' of 7351 Å³ or 8.7 % each. The overall void volume is 14750 Å³ or 17 % of the unit cell volume (84656 Å³), when calculated using solvent molecule of diameter of 1.4 Å. There is a continuous single channel

running along the *a/c* axes[22] (Figure S2) with the narrowest region accommodating a probe molecule radius of 2 Å³ with the other two dimensions of about 1.4×1.6 nm. Within the channels there is no fixed ordering of solvent based on the residual electron density maps. The thermal stability of **HOF-3COOH** building block measured by the TGA curve under N_2 (Figure S9) experienced an initial 5 % weight loss below 80 °C, attributed to the loss of solvent within the

pores. A second weight loss of >20% between 200°C and 600°C was attributed to any remaining solvent trapped and the thermal decomposition of the molecular precursors. The CO_2 adsorption isotherm at 223 K of **HOF-3COOH** shows an uptake capacity of 3.28 mmol/g (Figure S10), which can be considered excellent for a HOF.[5,24] Next, **HOF-3COOH** crystals were immersed in a warm solution of **TPY** in toluene (0.6 mg/mL) and the solvent was left to evaporate at a slow rate (~18 hours), yielding HOF-on-HOF crystals of **HOF-3COOH@P2-TPY**. SEM confirmed the core–shell morphology of **P2-TPY** as nanometric crystalline rods (Figure 4d) growing on the surface of **HOF-3COOH**. EDS analysis of **HOF-3COOH@P2-TPY** for C, N and O elements showed the presence of C and N at the shell and only C and O at the solid core of the crystal (Figure 4e–f, Figure S11). PXRD also confirmed the presence of the **P2-TPY** phase and the maintained integrity of **HOF-3COOH** phase, (Figure S12–S13). FTIR analysis of **HOF-3COOH@P2-TPY** crystals confirmed the presence of characteristic peaks of **P2-TPY** and **HOF-3COOH** (Figure S14). The dissimilar parameters for the unit cells in both crystals ($a = 54.6$ Å, $b = 31.2$ Å, $c = 54.5$ Å, $\beta = 114.6$ Å vs $a = 17.4$ Å, $b = 40.0$ Å, $c = 17.4$ Å, $\beta = 119.9$ Å) suggest a lattice mismatch. To shed light on the driving force for the core–shell formation, and the possible types of interactions at the interface, we co-crystallized **3COOH** and **TPY** obtaining crystals (**Hybrid-1**) that were characterized by SCXRD (Table S3). The crystals of **Hybrid-1** revealed an asymmetric unit consisting of seven pairs of **3COOH** molecules forming hydrogen bonds to **TPY** in a 1:1 ratio (more detailed description of the crystal packing in the SI). H-bonding interactions are observed between all three arms of **TPY** and **3COOH** through the N pyridyl acceptor and OH carboxyl donor atoms (2.49 Å average) (Figure S3). The presence of H-bonding interactions is not surprising, as numerous studies have demonstrated the stability of H-bonds between pyridine and carboxylic groups.[23] Further stabilizing interactions consisted of π–π stacking interactions between the central triazine ring, central phenyl rings and outer pyridyl rings with a step of around 3.34 Å between the planes.

Based on the crystal data obtained for **Hybrid-1**, **HOF-3COOH** and **P2-TPY**, we calculated the energy of H-bonding interactions between pairs. DFT calculations were performed using version 5.0.3 of the ORCA program.[25] The range-separated hybrid functional, ωB97X, was used to approximate the exchange–correlation functional. The polarized triple-zeta basis set, def2-TZVP,[26] as well as the general auxiliary basis, Def2/J,[27] were used in the calculations. The values in energy for both contributions, H-bonding and π–π stacking, account for 12 kcal/mol and 27 kcal/mol, respectively. The H-bond interaction calculation was repeated using the M06-2X functional so that this result can be directly compared with previous work.[21] The obtained energy value is very similar at 11.1 kcal/mol for the H-bond interaction on the co-crystals of **Hybrid-1** for COOH….N. This is significantly higher than the H-bond value of 5.4 kcal/mol for N….N in **P2-TPY** seen in previous works.[21] This suggests that the driven mechanism of growth

of **P2-TPY** on the surface of **HOF-3COOH** would be the stronger H-bond interactions that originated at the interface between **TPY** and **3COOH** crystals. The thermal stability of **HOF-3COOH@P2-TPY** building blocks was also studied by TGA under N_2. The TGA curve (Figure S17) experienced an initial 8% weight loss below 100°C, attributed to the loss of solvents within the pores. A second weight loss of >50% between 200°C and 450°C was attributed to any remaining solvent trapped within the pores and the thermal decomposition of the molecular precursors. The porosity of **HOF-3COOH@P2-TPY** was also studied by gas adsorption after sample activation (Figure S18). The CO_2 adsorption isotherm at 223 K of **HOF-3COOH@P2-TPY** shows an uptake capacity of 2.3 mmol/g, which it is expected, corresponding to an intermediate adsorption between both HOFs. To our knowledge, this is the first stable HOF-on-HOF crystal and the first POMM using dissimilar building blocks.[16]

Superhydrophobicity, Hierarchy, and Contaminant Trapping

Hierarchy in HOFs could be used as an elegant route for the introduction of multifunctionality in crystalline materials for specific applications. For example, the multiscale nature of some of these materials could be used to introduce special wettability and trapping properties. Previous studies have demonstrated that hierarchical materials can alter the surface's wettability.[28] However, the wettability of HOFs has been hardly explored, with only a few reports published, showing the amphiphilic nature of building blocks due to the presence of aromatic hydrophobic blocks and hydrophilic functional groups.[29–31] To increase the hydrophobic nature of HOFs, previous reports were based on designing fully fluorinated pores.[29] We propose that multiscale HOFs could be good candidates as hydrophobic materials. Some of these hierarchical materials display low wettability in the presence of water, forming liquid marbles and floating on water (Figure S19a). In fact, when we measured the contact angle for **P2-TPY@P2-TPY** crystals, angles of >150° were obtained, which can be considered as superhydrophobic (Figure 5a). To our knowledge, this is the first reported HOF with superhydrophobic properties. The high hydrophobicity was also demonstrated for **DFA-TPY** (Figure 5b) and **HOF-3COOH@P2-TPY** (Figure S19b). The hydrophobicity and hierarchical fractal nature of **DFA-TPY** could be advantageous in applications for challenging separations such as selective oil-water adsorption and microplastics trapping, as they are two of the most relevant environmental contaminants. Oil in water is a well-known and persistent contaminant[32] and, similarly, microplastics can be found in the environment and even the human body, with the toxicity that entails.[33] Traditional methods for the removal of microplastics in wastewater plants are not effective[34] and new methods are required.[35,36]

As a proof of concept, we tested **DFA-TPY** for the removal of both oil and solid contaminants from water. When a mixture of water and hexane or petroleum ether (Figure 5c) dyed with Oil Red were prepared, **DFA-TPY** was able to completely remove 99% of the oil in minutes,
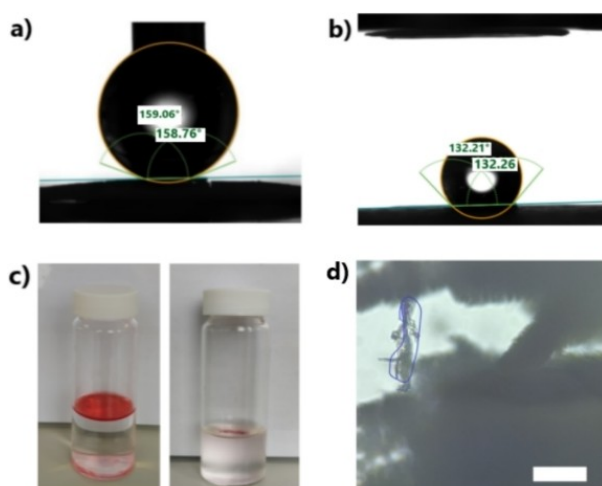
Figure 5. a–b) Contact angle measurements for **P2-TPY@ P2-TPY** (a) and **DFA-TPY** (b). c) Images of oil in water dyed with Oil Red before (left) and after adding **DFA-TPY** (right). d) Optical microscopy image of **DFA-TPY** with trapped microplastic after filtration. Scale bar: 10 μm.

proving the efficacy of hydrophobicity, with no visual evidence of remaining oil. For microplastics, a water solution containing PET microplastics was filtered through **DFA-TPY**, with 98 % of the total amount of microplastics removed. These efficacies for the capture of oil and microplastics are comparable with the state-of-the-art materials for both applications.[37,38] The mechanism of microplastic trapping is expected to be favored by hydrophobic interactions and the hierarchical nature of the fractal **DFA-TPY** (Figure 5d). Beyond its efficiency in removing contaminants and due to its crystalline nature, **DFA-TPY** can be easily regenerated and after the end of its life, recrystallized and reused again.

Conclusion

The ability to prepare crystalline organic porous materials with hierarchical superstructures is a current challenge in the field of POMMs, and particularly in HOFs. Herein, we have introduced the first examples of organic superstructures based on HOFs by using a controlled and sequential crystallization strategy, without the need of using templates or surface functionalization. We also demonstrated the potential of these superstructures to confer superhydrophobicity and trapping abilities for the capture of persistent water contaminants such as oils and microplastics. This work deepens our understanding of multiscale hierarchies, opening an avenue to design multifunctional HOFs such as HOF-on-HOF structures, where this strategy could serve of inspiration for the construction of more intricate multiscale and heterogeneous porous organic materials with optimized properties, as well as greatly expanding the library of HOF materials.

Supporting Information

The authors have cited additional references within the Supporting Information.[21,39–41]

Conflict of Interest

The authors declare no conflict of interest.

Data Availability Statement

The data that support the findings of this study are available from the corresponding author upon reasonable request. Supplementary crystallographic data for this paper are provided free of charge by the joint Cambridge Crystallographic Data Centre.[42]

Keywords: contaminant trapping · porous organic molecular materials · hierarchical assembly · hydrogen-bonded organic frameworks · superhydrophobicity

[1] M. A. Little, A. I. Cooper, *Adv. Funct. Mater.* **2020**, *30*, 1909842.

[2] I. Hisaki, C. Xin, K. Takahashi, T. Nakamura, *Angew. Chem. Int. Ed.* **2019**, *58*, 11160–11170.

[3] K. Geng, R. Liu, S. Dalapati, S. Dalapati, K. T. Tan, Z. Li, S. Tao, Y. Gong, Q. Jiang, D. Jiang, *Chem. Rev.* **2020**, *16*, 8814–8933.

[4] Q. Wang, D. Astruc, *Chem. Rev.* **2020**, *2*, 1438–1511.

[5] R.-B. Lin, Y. He, P. Li, H. Wang, W. Zhou, B. Chen, *Chem. Soc. Rev.* **2019**, *48*, 1362–1389.

[6] P. J. Santos, P. A. Gabrys, L. Z. Zornberg, M. S. Lee, R. J. Macfarlane, *Nature* **2021**, *591*, 586–591.

[7] H. Han, S. Kallakuri, Y. Yao, C. B. Williamson, D. R. Nevers, B. H. Savitzky, R. S. Skye, M. Xu, O. Voznyy, J. Dshemuchadse, L. F. Kourkoutis, S. J. Weinstein, T. Hanrath, R. D. Robinson, *Nat. Mater.* **2022**, *21*, 518–525.

[8] Y. Luo, M. Ahmad, A. Schug, M. Tsotsalas, *Adv. Mater.* **2019**, *31*, 1901–744.

[9] L. Feng, K.-Y. Wang, J. Willman, H.-C. Zhou, *ACS Cent. Sci.* **2020**, *3*, 359–367.

[10] L. Feng, K.-Y. Wang, J. Powell, H.-C. Zhou, *Matter* **2019**, *4*, 801–824.

[11] Q. Tang, G. Zhang, B. Jiang, D. Ji, H. Kong, K. Riehemann, Q. Ji, H. Fuchs, *SmartMat.* **2021**, *2*, 109–118.

[12] P. Bairi, K. Minami, W. Nakanishi, *ACS Nano* **2016**, *10*, 6631–6637.

[13] Y. Lei, S. Wang, Z. Lai, X. Yao, Y. Zhao, H. Zhang, H. Chen, *Nanoscale* **2019**, *11*, 8692.

[14] J. F. Soria, A. Fernandez, *Nano-Micro Lett.* **2024**, *16*: 88.

[15] Q. Lv, X.-D. Wang, L.-S. Liao, *Adv. Funct. Mater.* **2022**, *32*, 2202364.

[16] S. Jiang, Y. Du, M. Marcello, E. W. Corcoran Jr, D. C. Calabro, S. Y. Chong, L. Chen, R. Clowes, T. Hasell, A. I. Cooper, *Angew. Chem. Int. Ed.* **2018**, *57*, 11228–11232.

[17] B.-T. Liu, X.-H. Pan, D.-Y. Zhang, R. Wang, J.-Y. Chen, H.-R. Fang, T.-F. Liu, *Angew. Chem. Int. Ed.* **2021**, *60*, 25701–25707.

[18] Z. Feng, T. Hai, Y. Liang, Q. Zhang, Y. Lei, *Angew. Chem. Int. Ed.* **2021**, *60*, 27046–27052.

[19] M. Hua, J. Hao, Y. Gong, F. Zhang, J. Wei, Z. Yang, M.-P. Pileni, *ACS Nano* **2020**, *14*, 5517–5528.

[20] J. Wang, Y. Mao, R. Zhang, Y. Zeng, C. Li, B. Zhang, J. Zhu, J. Ji, D. Liu, R. Gao, Y. Ma, *Adv. Sci.* **2022**, *9*, 2204036.

[21] C. A. Halliwell, S. E. Dann, J. Ferrando-Soria, F. Plasser, K. Yendall, E. V. Ramos-Fernandez, G. T. Vladisavljević, M. R. J. Elsegood, A. Fernandez, *Angew. Chem. Int. Ed.* **2022**, *134*, e202208677.

[22] D. H. Juers, J. Ruffin, *J. Appl. Crystallogr.* **2014**, *47*, 2105–2108.

[23] A. M. Beatty, *Coord. Chem. Rev.* **2003**, *246*, 131–143.

[24] C. A. Zentner, H. W. H. Lai, J. T. Greenfield, R. A. Wiscons, M. Zeller, C. F. Campana, O. Talu, S. A. FitzGeralde, J. L. C. Rowsell, *Chem. Commun.* **2015**, *51*, 11642.

[25] F. Neese, *Wiley Interdiscip. Rev.: Comput. Mol. Sci.* **2012**, *2*, 73–78.

[26] F. Weigend, R. Ahlrichs, *Phys. Chem. Chem. Phys.* **2005**, *7*, 3297.

[27] F. Weigend, *Phys. Chem. Chem. Phys.* **2006**, *8*, 1057.

[28] B. Su, Y. Tian, L. Jiang, *Chem. Rev.* **2015**, *115*, 8230–8293.

[29] T.-H. Chen, I. Popov, W. Kaveevivitchai, *Nat. Commun.* **2014**, *5*, 5131.

[30] Z.-M. Ye, X.-W. Zhang, P.-Q. Liao, Y. Xie, Y.-Tong Xu, X.-F. Zhang, C. Wang, D.-X. Liu, N.-Y. Huang, Z.-H. Qiu, D.-D. Zhou, C.-T. He, J.-P. Zhang, *Angew. Chem. Int. Ed.* **2020**, *59*, 23322–23328.

[31] Y.-H. Luo, X.-T. He, D.-L. Hong, C. Chen, F.-H. Chen, J. Jiao, L.-H. Zhai, L.-H. Guo, B.-W. Sun, *Adv. Funct. Mater.* **2018**, *28*, 1804822.

[32] D. Kawecki, B. Nowack, *Environ. Sci. Technol.* **2019**, *53*, 9664–9676.

[33] M. Afzal, K. Rehman, G. Shabir, *npj Clean Water* **2019**, *2*, 3.

[34] V. K. Gupta, I. Ali, T. A. Saleh, A. Nayak, S. Agarwal, *RSC Adv.* **2012**, *2*, 6380–6388.

[35] X. Fu, S. Zhang, X. Zhang, Y. Zhang, B. Li, K. Jin, X. Feng, J. Hong, X. Huang, H. Cao, Q. Yuan, P. Ai, H. Yu, Q. Li, *Adv. Funct. Mater.* **2023**, *33*, 2212570.

[36] M. Sarcletti, H. Park, J. Wirth, S. Englisch, A. Eigen, D. Drobek, D. Vivod, B. Friedrich, R. Tietze, C. Alexiou, D. Zahn, B. A. Zubiri, E. Spiecker, M. Halik, *Mater. Today* **2021**, *48*, 38–46.

[37] S. Ozden, S. Monti, V. Tozzini, N. S. Dutta, S. Gili, N. Caggiano, A. J. Link, N. M. Pugno, J. Higgins, R. D. Priestley, C. B. Arnold, *Mater. Today* **2022**, *59*, 46–55.

[38] L.-H. Xie, M.-M. Xu, X.-M. Liu, M.-J. Zhao, J.-R. Li, *Adv. Sci.* **2020**, *7*, 1901758.

[39] CrysAlisPRO, Oxford Diffraction /Agilent Technologies UK Ltd, Yarnton, England.

[40] L. J. Bourhis, O. V. Dolomanov, R. J. Gildea, J. A. K. Howard, H. Puschmann, *Acta Crystallogr.* **2015**, *A71*, 59–75.

[41] F. Neese, *WIREs Comput. Mol. Sci.* **2022**, *12*, e1606.

[42] Deposition numbers CCDC 2311256 for **P2-TPY**, 2304619 for **Hybrid-1** and 2306105 for **HOF-3COOH** contain the supplementary crystallographic data for this paper.